

**Flat-band transport and Josephson effect through a finite-size sawtooth lattice**

Ville A. J. Pyykkönen <sup>1</sup>, Sebastiano Peotta <sup>1,2,3</sup>, Philipp Fabritius <sup>4</sup>,  
 Jeffrey Mohan <sup>4</sup>, Tilman Esslinger <sup>4</sup> and Päivi Törmä <sup>1,\*</sup>

<sup>1</sup>*Department of Applied Physics, Aalto University School of Science, FI-00076 Aalto, Finland*

<sup>2</sup>*Computational Physics Laboratory, Physics Unit, Faculty of Engineering and Natural Sciences, Tampere University, FI-33014 Tampere, Finland*

<sup>3</sup>*Helsinki Institute of Physics, University of Helsinki, FI-00014 Helsinki, Finland*

<sup>4</sup>*Department of Physics, ETH Zurich, 8093 Zurich, Switzerland*



(Received 12 January 2021; accepted 13 April 2021; published 28 April 2021)

We study theoretically the transport through a finite-size sawtooth lattice coupled to two fermionic reservoirs kept in the superfluid state. We focus on the DC Josephson effect and find that the flat-band states of the sawtooth lattice can support larger critical current and a higher temperature than the dispersive band states. However, for this to occur the boundary states of the finite-size lattice need to be tuned at resonance with the bulk flat-band states by means of additional boundary potentials. We show that transport in a two-terminal configuration can reveal the salient features of the geometric contribution of flat-band superconductivity, namely the linear dependence of key quantities, such as the critical current and critical temperature, on the interaction. Our results are based on parameters of a realistic experimental lattice potential, and we discuss the conditions one needs to reach to observe the predicted effects experimentally.

DOI: [10.1103/PhysRevB.103.144519](https://doi.org/10.1103/PhysRevB.103.144519)

**I. INTRODUCTION**

A flat band is a Bloch band of a lattice model which is dispersionless, usually as a consequence of destructive quantum interference between alternative hopping paths. This means that all the states in the band are degenerate and localized, while the kinetic energy of noninteracting particles is completely quenched. The massive degeneracy of flat bands leads to the strongly-correlated regime and new emergent phases as soon as interparticle interactions are switched on [1]. Indeed, at the theoretical level, flat bands have been proposed to host ferrimagnetic [2] and ferromagnetic phases [3–7], various topological states [8–12], Wigner crystallization [13], and superconductivity, the main focus of this work. Lattice models with flat bands can be realized experimentally with optical lattices for ultracold atoms [14–16], photonic lattices [17–21], polaritons [22], but also in van der Waals materials [23–26] and artificial electronic systems [27–29].

Flat bands potentially enable high temperature superconductivity, up to room temperature [30–32]. It has been shown theoretically that superconductivity occurs in flat bands in the presence of attractive interactions only if the band has a nontrivial quantum metric [33–35], which is an invariant of the band structure related to the Berry curvature. More specifically, it has been found that in the flat-band limit the geometric contribution of superconductivity [33] dominates and the superfluid weight is *linearly proportional* to both the coupling constant of the attractive interparticle interaction and the integral of the quantum metric over the first Brillouin

zone. A nonzero superfluid weight is the defining property of superfluid/superconducting states.

Predictions of flat-band superconductivity are supported by the recent remarkable discovery of superconductivity in magic-angle twisted bilayer graphene [23], which is believed to be a direct consequence of the nearly flat bands that occur in the band structure at a specific (“magic”) twist angle between the two graphene layers. Indeed, it has been shown in three distinct theoretical studies [36–39] that the geometric contribution to the superfluid weight, that is the part of the superfluid weight proportional to the band quantum metric, is important in magic-angle twisted bilayer graphene. However, this evidence is only indirect since twisted bilayer graphene is a complex material and some important questions are still open, such as the origin of the attractive interaction responsible for superconductivity [40,41]. Moreover, the degree of control on the material properties achieved on this material, for instance by tuning the twist angle, is outstanding but still too limited to provide direct evidence of the effects associated with the flat-band quantum metric. An experiment taking advantage of the degree of control available in ultracold gas experiments [42] is a highly promising platform for investigating the role played by quantum geometry in a flat-band superfluid, as for instance the interaction can be tuned to verify the expected linear dependence of the geometric contribution of superconductivity on interaction.

In order to study flat-band superconductivity in the ultracold gas context, we propose and simulate here an atomtronic two-terminal transport setup in which a finite-size sawtooth lattice is placed in contact at the two ends with two superfluid fermionic reservoirs. A similar sawtooth lattice model has been studied in the case of noninteracting particles in

\*paivi.torma@aalto.fi

Ref. [43], where the focus was on adiabatic pumping, and in Ref. [44] in the context of nonlinear localized modes. A sawtooth lattice has been also investigated in the context of photonic lattices both experimentally and theoretically in Ref. [20]. Two-terminal transport setups are commonly employed to probe solid state mesoscopic systems [45] and more recently transport experiments of this kind have been realized also using ultracold fermionic lithium atoms [46–50]. In this way the quantization of conductance has been observed in neutral matter for the first time [47]. The main goal of atomtronics [51,52] is to achieve a high degree of control on ultracold atom transport and ultimately realize complex working devices as in electronics.

Ultracold atoms offer new possibilities with no counterpart in electronics. Two are particularly important for the present work: first, the control on interatomic interactions by means of Feshbach resonances and, second, the ability to flexibly engineer complex lattice potentials in the region between the reservoirs (the “scattering region” in the Landauer picture of transport) using for instance a digital micromirror device (DMD) [49]. By tuning the interatomic interaction strength it should be possible to show that the superfluid weight is *linearly proportional to the interaction*, which is the fingerprint of the effect of the quantum metric on the superfluid properties. This is much harder to do in the solid state context since the interaction strength can be tuned only to a limited extent. Concerning the lattice potentials, digital micromirror devices or more traditional optical lattices can be used to realize complex potentials that implement lattice models with flat bands in the tight-binding limit. A viable optical lattice scheme has been proposed for instance in the case of the sawtooth ladder [53,54], which is the lattice model considered in this work.

In a two-terminal setup, it is only possible to insert a finite portion of an infinite lattice model in between the two reservoirs. This creates a nontrivial problem in the case of lattice models with flat bands, which has no counterpart for dispersive bands. The problem is due to the localized nature of the states which compose a flat band: When the infinite lattice is truncated, the flat-band states away from the ends of the finite system (the “bulk” states) are essentially unaffected precisely because they are strongly localized on a few lattice sites that are not directly connected to the boundary lattice sites by hopping matrix elements [55]. On the other hand, the few (usually two) flat-band states localized on lattice sites at the two ends of the finite system are strongly affected by the truncation and in general they are not anymore degenerate with the bulk states. These “boundary” states are essential for the current to flow from the reservoirs to the bulk of the finite-size system, thus the loss of degeneracy has usually the effect of dramatically suppressing transport through the flat band, as is shown in the following in the case of the sawtooth ladder. This is an effect specific to flat bands and it is not observed in the case of dispersive bands whose states have a delocalized, plane-wave-like character.

A key result of this work is that this problem can be solved by properly tuning the energy of the boundary states. Due to the localized character of the flat-band states, this can be easily done by introducing additional potential terms at the two ends, which have the purpose of restoring the degeneracy

between bulk and boundary states. We expect this problem to be present in various forms of transport, such as in the steady state when the system is driven out of equilibrium by a chemical potential difference. However, in this work we restrict ourselves to the case of transport at equilibrium between superfluid/superconducting reservoirs that is to the DC Josephson effect [56,57]. This is technically the simplest case to handle because the Josephson effect occurs at equilibrium in the presence of a phase difference between the two reservoirs. Moreover, it is more directly connected to previous results on the superfluid weight in infinite lattices [33–35]. Indeed, the superfluid weight is the coefficient of proportionality between the superfluid current and the phase gradient in the bulk [58,59], while the Josephson critical current is the coefficient of proportionality between the Josephson current and the phase bias in the limit of small bias. Thus, it is evident that the large superfluid weight in a flat band with nonzero quantum metric, as predicted in previous works [33,35,60], translates into an expected large Josephson critical current in a two-terminal setup. This expectation is fully confirmed in this work, under the condition that the degeneracy between boundary and bulk states is restored, as briefly explain above and with extensive details in the following. The Josephson effect, without any connection to flat-band physics, has been widely studied in ultracold gas experiments [61–68] and most recently observed in superfluid Fermi gas [69,70].

The paper is organized as follows. Section II A presents the model and in Sec. II B the method used to compute the Josephson current is described in detail. In Sec. III A, we first discuss results in the case when interactions are not present within the finite-size sawtooth lattice and then show how the Josephson current is modified by interactions. In Sec. III B we include the boundary potentials that allow us to restore the degeneracy between bulk and boundary states, as discussed above, and show that the Josephson current through the flat band is strongly enhanced at resonance. In Sec. III C we include the effect of a finite temperature and estimate the superconducting critical temperatures below which a nonzero Josephson critical current can be observed, both in the flat and dispersive band case. In Sec. IV a possible experimental realization with ultracold gases is proposed based on an optical potential that can be used to implement the sawtooth lattice. Finally, in Sec. V we discuss and summarize the results.

## II. METHODS

### A. Tight-binding model Hamiltonian

We consider a two-terminal setup comprising a finite portion of a sawtooth ladder and two leads (the reservoirs) described by the following noninteracting tight-binding Hamiltonian

$$\hat{H}_0 = \hat{H}_{\text{sawtooth}} + \hat{H}_L + \hat{H}_R + \hat{H}_{\text{contact}}, \quad (1)$$

where  $\hat{H}_{\text{sawtooth}}$  describes the sawtooth lattice,  $\hat{H}_L$ ,  $\hat{H}_R$  describe the two leads, left and right, respectively, and  $\hat{H}_{\text{contact}}$  describes the contact between leads and the sawtooth ladder. A sketch of a possible experimental setup is shown in Fig. 1(a). The tight-binding model is presented in Fig. 1(b), where the notation employed here is also introduced.

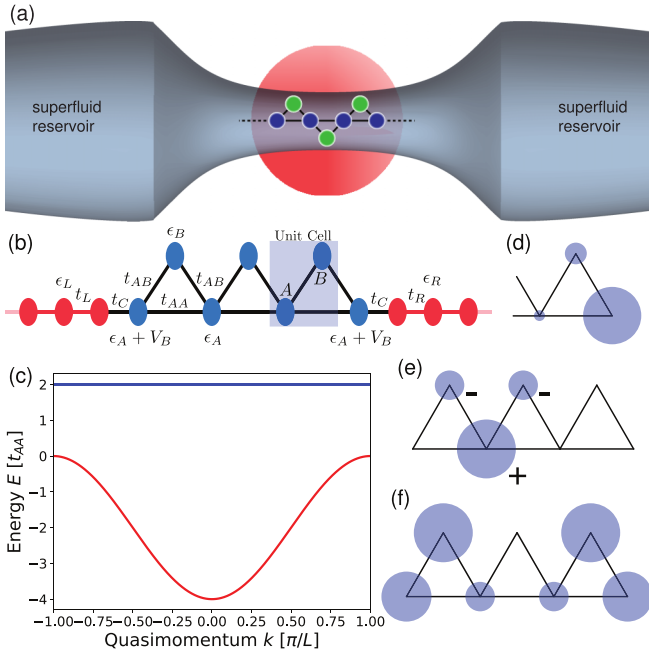


FIG. 1. (a) Sketch of the proposed two-terminal ultracold gas experiment [47,50]. The cigar shaped cloud of lithium 6 is divided into two reservoirs by a narrow constriction, where the sawtooth lattice is imprinted. The red region marks the gate beam used to control the chemical potential in the junction region. (b) Description of the two-terminal setup tight-binding model as a graph where the sites represent onsite energies and the edges the nonzero hopping amplitudes between sites. The figure introduces the notation and shows the structure of the sawtooth ladder and the leads. The leads (red sites) are semi-infinite. (c) The band structure of an infinite sawtooth ladder with parameters  $\epsilon_A = \epsilon_B = 0$ ,  $t_{AB} = \sqrt{2}t_{AA}$ . Figures (d)–(f) show examples of different eigenstate types of the finite-size sawtooth ladder. The sizes of the circles at the lattice sites indicate the wave-function amplitude squared, that is, the relative probabilities. (d) An edge state. (e) A flat-band state. The signs  $\pm$  denotes the respective phases of the wave function at the sites. (f) A dispersive band state.

The sawtooth ladder is a 1D lattice with two sites per unit cell, called  $A$  and  $B$  [53]. The  $A$  sites are connected to the nearest neighbor  $A$  sites by the hopping amplitude  $t_{AA}$  and to the nearest-neighbor  $B$  sites by  $t_{AB}$ . The  $B$  sites are not connected to each other by direct hopping amplitudes. At each site there is an onsite energy term  $\epsilon_A$ ,  $\epsilon_B$  for  $A$  and  $B$  sites, respectively. The sawtooth ladder Hamiltonian is

$$\begin{aligned} \hat{H}_{\text{sawtooth}} = & \sum_{i=1}^{N_c} \sum_{\sigma} [(\epsilon_A \hat{c}_{A,i\sigma}^{\dagger} \hat{c}_{A,i\sigma} + \epsilon_B \hat{c}_{B,i\sigma}^{\dagger} \hat{c}_{B,i\sigma}) \\ & - (t_{AB} \hat{c}_{B,i\sigma}^{\dagger} \hat{c}_{A,i\sigma} + t_{AB} \hat{c}_{A,i+1\sigma}^{\dagger} \hat{c}_{B,i\sigma} \\ & + t_{AA} \hat{c}_{A,i+1\sigma}^{\dagger} \hat{c}_{A,i\sigma} + \text{H.c.})] \\ & + \sum_{\sigma} \epsilon_A \hat{c}_{A,N+1\sigma}^{\dagger} \hat{c}_{A,N+1\sigma}, \end{aligned} \quad (2)$$

where  $N_c$  is the number of unit cells and  $\hat{c}_{\alpha,i\sigma}$ ,  $\hat{c}_{\alpha,i\sigma}^{\dagger}$  annihilates and creates, respectively, a particle at the site  $\alpha = A/B$  of unit cell  $i$  with spin  $\sigma = \{\uparrow, \downarrow\}$ .

The sawtooth ladder has two sites per unit cell so it contains two bands, one of which is flat if the hopping amplitudes satisfy the condition  $t_{AB} = \pm \sqrt{2t_{AA}^2 + (\epsilon_B - \epsilon_A)t_{AA}}$ , and the other is dispersive. We consider here the case  $\epsilon_A = \epsilon_B$  and  $t_{AB} = \sqrt{2}t_{AA}$ , which gives the band structure in Fig. 1(c). The sawtooth ladder tight-binding Hamiltonian with the leads removed possesses  $2N_c + 1$  eigenstates,  $N_c - 1$  of which are the flat-band states, 2 are edge states, also known as boundary states, and the rest  $N_c$  are related to the dispersive band. The localized flat-band states, where contributions outside a V shaped region vanish due to destructive interference, are shown in Fig. 1(e). Notice that the localized states shown in Fig. 1(e) are not orthogonal to each other. Nevertheless, the states span the flat-band subspace, and a proper orthonormal basis can be constructed comprising very similar states, which however possess exponentially decaying tails [53]. An example of a state of the dispersive band is shown in Fig. 1(f). The dispersive band states are spread over the whole system. An example of edge state is shown in Fig. 1(d). It has major contribution at one edge and decays exponentially as a function of distance from the edge.

The leads are modeled as simple chains with local onsite energy  $\epsilon_L$ ,  $\epsilon_R$  where  $L, R$  refer to left and right leads, respectively. The lead bandwidth is controlled by the hopping amplitude between sites  $t_{L/R}$ . The leads are connected to the sawtooth ladder at the edge  $A$  sites by contact hopping amplitudes  $t_C$ . The leads are modeled by the Hamiltonians

$$\hat{H}_{L/R} = \sum_{i,\sigma} [\epsilon_{L/R} \hat{c}_{L/R,i\sigma}^{\dagger} \hat{c}_{L/R,i\sigma} - t_{L/R} (\hat{c}_{L/R,i+1\sigma}^{\dagger} \hat{c}_{L/R,i\sigma} + \text{H.c.})], \quad (3)$$

where  $\hat{c}_{L/R,i\sigma}^{\dagger}$ ,  $\hat{c}_{L/R,i\sigma}$  are the creation and annihilation operators for the leads. The unit cell index  $i = \{1, 2, \dots\}$  in the lead operators increases from the edge. Finally, the contact Hamiltonian is

$$\begin{aligned} \hat{H}_{\text{contact}} = & \sum_{\sigma} [-t_C (\hat{c}_{L,1\sigma}^{\dagger} \hat{c}_{A,1\sigma} + \hat{c}_{R,1\sigma}^{\dagger} \hat{c}_{A,N+1\sigma} + \text{H.c.}) \\ & + V_B (\hat{c}_{A,1\sigma}^{\dagger} \hat{c}_{A,1\sigma} + \hat{c}_{A,N+1\sigma}^{\dagger} \hat{c}_{A,N+1\sigma})], \end{aligned} \quad (4)$$

where  $t_C$  is the tunneling amplitude between lead and the sawtooth lattice and  $V_B$  is a boundary potential introduced to tune the edge states energy and restore degeneracy as discussed in Sec. I.

## B. Interacting Hamiltonian and self-consistent mean field method

The full many-body grand canonical Hamiltonian takes the form

$$\hat{H} = \hat{H}_0 + \hat{H}_{\text{int}} - \mu \hat{N}, \quad (5)$$

where the interaction term  $\hat{H}_{\text{int}}$  is the Hubbard interaction

$$\hat{H}_{\text{int}} = - \sum_i U_{\alpha} \hat{c}_{\alpha,i\uparrow}^{\dagger} \hat{c}_{\alpha,i\uparrow} \hat{c}_{\alpha,i\downarrow}^{\dagger} \hat{c}_{\alpha,i\downarrow}, \quad (6)$$

$\mu$  is the chemical potential, and  $\hat{N} = \sum_{\alpha,i\sigma} \hat{c}_{\alpha,i\sigma}^{\dagger} \hat{c}_{\alpha,i\sigma}$  is the number operator. Here the index  $\alpha = \{L, R, A, B\}$  labels the various parts of the system,  $U_{\alpha} \geq 0$  (attractive interaction) is the interaction strength, and  $i$  goes over the unit cells of

the tight-binding model. To solve the many-body problem, we use the Bardeen-Cooper-Schrieffer (BCS) mean-field theory in the form of the Bogoliubov-Valatin canonical transformation. In the case of flat bands, the mean-field theory is expected to perform well for interaction strengths  $U_\alpha$  up to the band gap between the flat band and its nearest neighboring band [71]. The band gap between the flat band and the dispersive band in the sawtooth lattice is  $2t_{AA}$ . In the mean field approximation, we approximate the Hubbard term as follows, up to a constant

$$U_\alpha \hat{c}_{\alpha,i\uparrow}^\dagger \hat{c}_{\alpha,i\uparrow} \hat{c}_{\alpha,i\downarrow}^\dagger \hat{c}_{\alpha,i\downarrow} \simeq U_\alpha \left( \langle \hat{c}_{\alpha,i\uparrow}^\dagger \hat{c}_{\alpha,i\uparrow} \rangle \hat{c}_{\alpha,i\downarrow}^\dagger \hat{c}_{\alpha,i\downarrow} + \langle \hat{c}_{\alpha,i\downarrow}^\dagger \hat{c}_{\alpha,i\downarrow} \rangle \hat{c}_{\alpha,i\uparrow}^\dagger \hat{c}_{\alpha,i\uparrow} + \langle \hat{c}_{\alpha,i\uparrow}^\dagger \hat{c}_{\alpha,i\downarrow}^\dagger \rangle \hat{c}_{\alpha,i\downarrow} \hat{c}_{\alpha,i\uparrow} + \langle \hat{c}_{\alpha,i\downarrow}^\dagger \hat{c}_{\alpha,i\uparrow} \rangle \hat{c}_{\alpha,i\uparrow}^\dagger \hat{c}_{\alpha,i\downarrow} \right). \quad (7)$$

By utilizing the canonical commutation relations, we write the system Hamiltonian in Nambu form with the vectors

$$\hat{d}_{\alpha,i} = \begin{pmatrix} \hat{c}_{\alpha,i\uparrow} \\ \hat{c}_{\alpha,i\downarrow}^\dagger \end{pmatrix}, \quad \hat{d}_{\alpha,i}^\dagger = (\hat{c}_{\alpha,i\uparrow}^\dagger \quad \hat{c}_{\alpha,i\downarrow}). \quad (8)$$

In this basis, we have up to a constant

$$\hat{H} \simeq \sum_{\alpha i, j\beta} \hat{d}_{\alpha,i}^\dagger \mathcal{H}_{\text{BdG},\alpha i, \beta j} \hat{d}_{\beta,j}, \quad (9)$$

where we have defined the Bogoliubov-de Gennes (BdG) Hamiltonian  $\mathcal{H}_{\text{BdG}}$  as

$$\mathcal{H}_{\text{BdG},\alpha i, \beta j} = \begin{pmatrix} T_{\alpha i, \beta j} + V_{\alpha i\downarrow} \delta_{\alpha i, \beta j} & \Delta_{\alpha i} \delta_{\alpha i, \beta j} \\ \Delta_{\alpha i}^* \delta_{\alpha i, \beta j} & -T_{\alpha i, \beta j} - V_{\alpha i\uparrow} \delta_{\alpha i, \beta j} \end{pmatrix}. \quad (10)$$

Here

$$T_{\alpha i, \beta j} = (\epsilon_{\alpha, i} - \mu) \delta_{\alpha i, \beta j} - t_{\alpha i, \beta j} \quad (11)$$

includes all of the single-particle terms of the grand canonical Hamiltonian (5), the superconducting order parameter  $\Delta_{\alpha i}$  is given by the gap equation

$$\Delta_{\alpha i} = -U_\alpha \langle \hat{c}_{\alpha, i\downarrow} \hat{c}_{\alpha, i\uparrow} \rangle \quad (12)$$

and the Hartree potential  $V_{\alpha i\sigma}$  is given by

$$V_{\alpha i\uparrow/\downarrow} = -U_\alpha \langle \hat{c}_{\alpha, i\downarrow/\uparrow}^\dagger \hat{c}_{\alpha, i\downarrow/\uparrow} \rangle. \quad (13)$$

In this work, we assume time-reversal symmetry which implies  $V_{\alpha i\uparrow} = V_{\alpha i\downarrow} \equiv V_{\alpha i}$ .

The mean-field BdG Hamiltonian is diagonalized as  $\mathcal{H}_{\text{BdG}} = SDS^\dagger$ , where  $D$  is a diagonal matrix containing the eigenvalues of  $\mathcal{H}_{\text{BdG}}$  and  $S$  is the unitary matrix comprising the corresponding eigenvectors as columns, in the respective order. In the diagonalized basis, the Hamiltonian becomes

$$\hat{H} = \sum_{n\sigma} E_n \hat{\gamma}_{n\sigma}^\dagger \hat{\gamma}_{n\sigma} \quad (14)$$

where  $E_n$  are the eigenvalues contained in  $D$  and the quasiparticle operators  $\gamma_{n\sigma}$  are defined by the following

Bogoliubov-Valatin transformations

$$\begin{aligned} \hat{c}_{\alpha, i\uparrow} &= \sum_n (u_{\alpha i, n} \hat{\gamma}_{n\uparrow} + v_{\alpha i, n}^* \hat{\gamma}_{n\downarrow}^\dagger) \\ \hat{c}_{\alpha, i\downarrow}^\dagger &= \sum_n (v_{\alpha i, n} \hat{\gamma}_{n\uparrow}^\dagger - u_{\alpha i, n}^* \hat{\gamma}_{n\downarrow}^\dagger), \end{aligned} \quad (15)$$

with coefficients  $u_{\alpha i, n}$ ,  $v_{\alpha i, n}$  given by  $u_{\alpha i, n} = S_{2(\alpha i)-1, n}$ ,  $v_{\alpha i, n} = S_{2(\alpha i), n}$  related to positive eigenenergies  $E_n$ , where  $\alpha i = \{1, 2, \dots\}$  denotes the index corresponding to the site of unit cell  $i$  in sublattice  $\alpha$  in the indexing of the single-particle Hamiltonian matrix (11). In the mean-field approximation, the quasiparticles are noninteracting and thus obey the Fermi-Dirac statistics.

Using the Bogoliubov-Valatin transformation in Eq. (12), one obtains the gap equation

$$\Delta_{\alpha i} = U_\alpha \sum_n u_{\alpha i, n} v_{\alpha i, n}^* \tanh\left(\frac{\beta E_n}{2}\right), \quad (16)$$

where  $E_n$  is the energy of the respective BdG Hamiltonian eigenstate  $n$  and  $\beta = 1/T$  is the inverse temperature (in our units Boltzmann's constant  $k_B = 1$ ) and similarly the Hartree potential is given by

$$V_{\alpha i} = - \sum_n \left( \frac{U_\alpha |u_{\alpha i, n}|^2}{\exp(\beta E_n) + 1} + \frac{U_\alpha |v_{\alpha i, n}|^2}{\exp(-\beta E_n) + 1} \right). \quad (17)$$

In the leads, the order parameters  $\Delta_{L/R, i}$  are set to a constant  $\Delta_L$ , while the Hartree potential  $V_{L/R, i}$  are put to zero. The finite Josephson current is the result of having the lead superconducting order parameters equal in amplitude but with different phases.

The order parameters  $\Delta_{A/B, i}$  and the Hartree potentials  $V_{A/B, i}$  are calculated self-consistently. In practice, the values for the self-consistent parameters are determined by the following iterative algorithm.

(1) Give initial guesses for the self-consistent parameters  $\Delta_{\alpha i}$  and  $V_{\alpha i}$ .

(2) Diagonalize the BdG Hamiltonian  $\mathcal{H}_{\text{BdG}}$ .

(3) Update the self-consistent parameters  $\Delta_{\alpha i}$  and  $V_{\alpha i}$  by using Eqs. (16) and (17) and the eigenvalues and eigenvectors of the BdG Hamiltonian obtained in step 2.

(4) If the difference between the updated and the pre-update parameters is less than the wanted accuracy (in an appropriate norm), end the procedure. Otherwise, go back to step 2.

Oftentimes this naive iterative procedure does not converge, leading to an oscillating solution. This issue can be solved by adopting a mixing algorithm, where self-consistent parameters of previous iterations are mixed at the Step 3 with the new values to give the update. For small enough mixing of the new iterate, the algorithm converges [72]. However, the convergence can be arbitrarily slow in general. To boost the convergence, we use two algorithms in combination with the simple mixing: the Broyden's method [73], which is a pseudo-Newton iteration, and the Anderson-Pulay mixing [74,75].

The current expectation value is obtained from the Heisenberg equation of motion for the particle number operator

$\hat{n}_{\alpha,i} = \sum_{\sigma} \hat{c}_{\alpha,i\sigma}^{\dagger} \hat{c}_{\alpha,i\sigma}$ , which leads to

$$\frac{dn_{\alpha i}}{dt} = \sum_{\beta j} I_{\alpha i, \beta j} + K_{\alpha i}, \quad (18)$$

where  $n_{\alpha i} = \langle \hat{n}_{\alpha i} \rangle$  is the particle number expectation value at orbital  $\alpha$  of unit cell  $i$  and

$$I_{\alpha i, \beta j} = \frac{i}{\hbar} \sum_{\sigma} t_{\alpha i, \beta j} (\langle \hat{c}_{\alpha, i\sigma}^{\dagger} \hat{c}_{\beta, j\sigma} \rangle - \langle \hat{c}_{\beta, j\sigma}^{\dagger} \hat{c}_{\alpha, i\sigma} \rangle) \quad (19)$$

$$K_{\alpha i} = \frac{i}{\hbar} (\Delta_{\alpha i}^* \langle \hat{c}_{\alpha, i\downarrow} \hat{c}_{\alpha, i\uparrow} \rangle - \Delta_{\alpha i} \langle \hat{c}_{\alpha, i\uparrow}^{\dagger} \hat{c}_{\alpha, i\downarrow}^{\dagger} \rangle), \quad (20)$$

where  $I_{\alpha i, \beta j}$  is the current expectation value from site  $\beta j$  to site  $\alpha i$ , and  $K_{\alpha i}$  is a source term. When the superconducting order parameter is calculated self-consistently,  $K_{\alpha i}$  vanishes and particle conservation is ensured since Eq. (18) becomes the usual continuity equation.

The leads are truncated to finite length so that the system is finite and closed, as in Ref. [76]. In the leads, however, the superconducting order parameter is constant and not calculated self-consistently, therefore  $K_{\alpha i}$  is finite and particle number is not conserved. This allows the system to sustain a finite equilibrium current even if it is closed. The Josephson current is obtained by evaluating expectation value in Eq. (19), which can be written in terms of the Bogoliubov-Valatin transformation parameters using

$$\langle \hat{c}_{\alpha, i\sigma}^{\dagger} \hat{c}_{\beta, j\sigma} \rangle = \sum_n \left( \frac{u_{\alpha i, n}^* u_{\beta j, n}}{e^{\beta E_n} + 1} + \frac{v_{\alpha i, n} v_{\beta j, n}^*}{e^{-\beta E_n} + 1} \right). \quad (21)$$

### III. RESULTS

#### A. Josephson current through a sawtooth ladder

We first present results for the Josephson current when  $U_{A/B} = 0$ , which we refer to as the noninteracting case, and then in the interacting case  $U_{A/B} \neq 0$ . Note that the leads are always assumed to be superconducting; the interactions necessary to induce superconductivity in the leads are not explicitly considered but are implicit in the constant superconducting order parameter of the leads. Thus noninteracting/interacting refers only to the sawtooth lattice in the transport channel. The noninteracting case is presented here because it is a useful reference for understanding the interacting case. Indeed, it illustrates how the various states of the finite-size sawtooth ladder affect the Josephson current.

We consider leads of 20 sites and a sawtooth ladder with  $N_c = 3$  unit cells. In order to make the results relevant for ultracold gas systems, the parameters for the sawtooth ladder tight-binding model are extracted from a realistic potential that can be realized experimentally with a digital micromirror device for instance, shown in Fig. 6. See Sec. IV for more details on a possible experimental realization. The lead parameters  $t_{L/R} = 30$  kHz are set so that the lead bandwidth is wide, that is, large in comparison to the other energy scales in the system. In Fig. 6 we collect all the sawtooth lattice parameters that are always fixed for the results presented here. The energy unit is the hertz (Hz) since we set  $\hbar = 1$ . This scale is appropriate for ultracold gas systems since 1 nK in temperature corresponds to 20.84 Hz and the usual temperatures are of order 60–70 nK [49,50]. The parameters not

specified in Figure 6 are varied in different analyses and provided separately. We always put a constant order parameter  $\Delta_L$  and zero Hartree potential  $V_L = 0$  in the leads, moreover in the noninteracting case the order parameter  $\Delta_{A/B}$  and Hartree potential  $V_{A/B}$  ladder vanish within the sawtooth ladder. The chemical potential  $\mu$  is tuned in order to control the filling of the states within the sawtooth ladder. For each value of the chemical potential, we vary the superconducting phase difference between the leads from 0 to  $2\pi$  and determine the maximal current, known as the critical Josephson current.

The noninteracting results at zero temperature are shown in Fig. 2(a). The critical Josephson current, that is, the maximal Josephson current with respect to the phase variation, is shown as a function of the chemical potential. As a comparison, the band structure of the infinite sawtooth ladder is shown for values of the energy corresponding to the chemical potential. It is seen that there are critical Josephson current peaks corresponding to the eigenstates of the finite size sawtooth ladder. Indeed, in the case of noninteracting particles at the junction, the transport through the lattice can be understood as being through the  $2N_c + 1$  eigenstates independently, each eigenstate behaving as a quantum dot. The literature on the transport through the quantum dots, including the Josephson transport, is vast [57,77]. The single state quantum dots present themselves in the Josephson current as peaks with varying chemical potential, the locations of which are dependent on the energy of the state/dot and the hopping amplitude between the leads and the dot. Furthermore, the form, width, and height of the peaks depend on the hopping amplitude and the order parameter at the leads  $\Delta_L$ . In the case of the noninteracting particles in the lattice system, the energies and the effective hopping amplitudes vary from state to state, explaining differences between the peaks. Importantly, the flat-band states are disconnected from the leads due to the fact that noninteracting particles are localized in the flat-band states, thus they do not give rise to any peak in the Josephson current. In agreement with this picture, we observe three peaks corresponding to the dispersive band and a peak corresponding to the two almost degenerate edge states. Also, as expected, there are no peaks corresponding to the flat-band state. We see that the positions of the peaks closely matches the band structure.

Next, we include interactions in the finite-size sawtooth ladder as well ( $U_A = U_B \neq 0$ ) and compute self-consistently the superconducting order parameter  $\Delta_{A/B, i}$  and the Hartree potential  $V_{A/B, i}$  as discussed in Sec. II B. The critical Josephson current as a function of the chemical potential is shown in Fig. 2(b). A new critical Josephson current peak is observed, which corresponds to the flat-band states. This agrees with the theoretical expectation based on the study of infinite lattice systems, since noninteracting particles are localized in flat bands but a finite interaction in geometrically nontrivial flat bands makes particles nonlocalized [33–35,78]. Furthermore, due to interactions, the current through all the states increases due to the increase of the pair potential by the interactions. Also, the peaks are shifted to lower chemical potential due to the Hartree potential. The widths and the shapes of the dispersive and boundary state peaks are also slightly modified in comparison to the noninteracting case. However, these changes are not qualitatively significant. The presence of a finite peak corresponding to the flat band is entirely an effect of

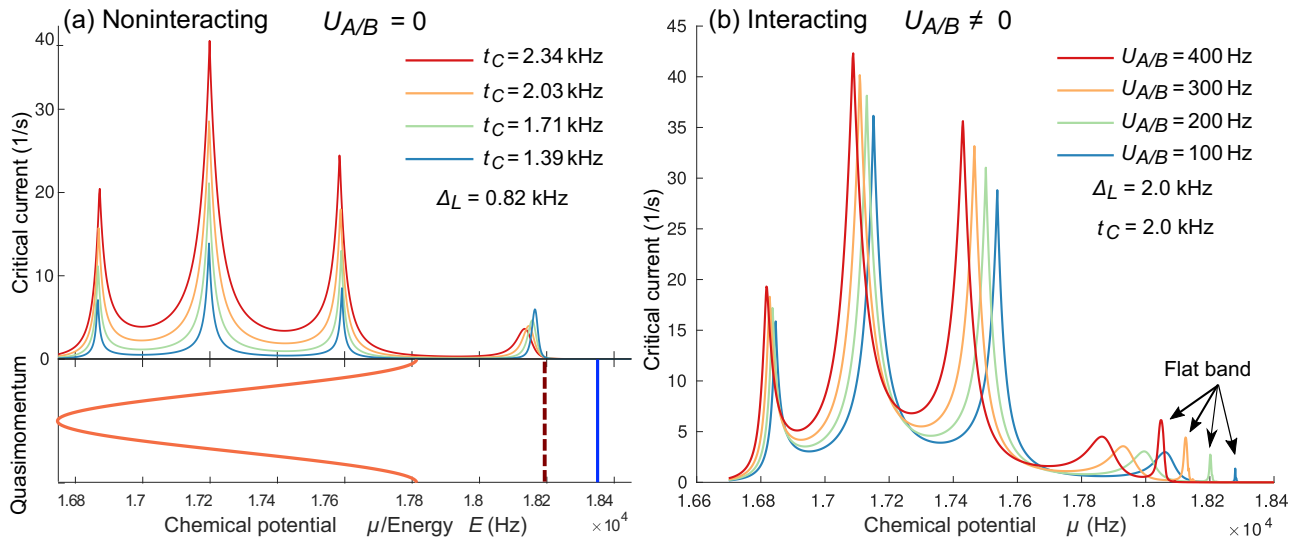


FIG. 2. (a) Critical Josephson current vs chemical potential  $\mu$  for a sawtooth ladder with  $N_c = 3$  unit cells without interactions ( $U_{A/B} = \Delta_{A/B,i} = V_{A/B,i} = 0$ ). In the lower panel, the band structure of an infinite sawtooth lattice, with the edge state energy indicated as a dashed line, is shown for comparison. The dispersive band states are responsible for the first three peaks from the left and are situated within the dispersive energy band of the infinite sawtooth ladder. There are  $N_c$  dispersive band states in a finite-size sawtooth ladder with  $N_c$  unit cells. The fourth peak is caused by the two almost degenerate edge states. The flat-band states (marked with blue in the dispersion relation) are not visible since noninteracting particles are localized in these states. (b) Critical Josephson current vs chemical potential through the interacting sawtooth ladder for various interaction strengths  $U_{A/B}$ . We observe the peaks of the same origin as in the noninteracting case of (a) and additionally a peak corresponding to the two bulk flat-band states [see Fig. 1(e)].

interactions, in line with the expectation that transport through flat-band states is especially sensitive to perturbations. The flat-band state peak critical Josephson current is found to be linearly dependent on the interaction strength  $U_{A/B}$  as can be expected from the linear dependence of the superfluid weight on the interaction strength in the case of an infinite lattice [33]. We observe that the flat-band state current peak is quite small in comparison to the current associated to dispersive band states even with interaction strength of the order of the band gap between the flat band and the dispersive band.

### B. Boundary potential

The observed flat-band state peak critical current in Fig. 2(b) is small in comparison to the critical currents through the dispersive band states. As we argued in Sec. I, the reason for this is the loss of degeneracy between bulk and edge states. In order to restore the degeneracy, we use the boundary potential  $V_B$  described in Sec. II A to tune the energy of the edge states. The effect of the edge state potential on the current is illustrated in Fig. 3. The parameters are the same as in the previous Sec. III A if not specified otherwise. It is seen that at a certain value of the edge potential  $V_B$ , the current is increased significantly with respect to the case  $V_B = 0$ . We have checked that at this value of the edge potential, the flat-band states and the edge states are degenerate. Thus, the hypothesis that the flat-band current is significantly increased when the edge states and flat-band states are degenerate seems to be correct. Importantly, the flat-band critical Josephson current is seen to increase *linearly* with the interaction strength in Fig. 3(c). We studied also the dependence of the flat-band state current on the length of the lattice. The results are shown in Fig. 4(a). It

is seen that, at the boundary potential resonance condition, the current dependence on the length (measured as the number of unit cells  $N_c$ ) follows a power law  $I \propto N_c^\alpha$  with  $\alpha \approx -1$ . This behavior is the one expected in the long junction limit [79,80] and is consistent with how the superconducting phase varies within the lattice, as shown in Fig. 4(b). It is seen that at the conditions of peak flat-band current, the critical current is achieved when the phase difference between the leads is close to  $\pi$ . Furthermore, the phase varies linearly from one lead to another. Since the Josephson current is proportional to the gradient of the phase, which is inversely proportional to the length of the lattice in the presence of a constant phase bias, the observed power law behavior of the current is obtained. Importantly, the order parameter amplitude  $|\Delta|$  at the peak flat-band current condition is seen to be roughly uniform within the junction. In contrast, at the off-peak condition also shown in Fig. 4(b), where dispersive band states are completely filled but the flat-band states are empty, the order parameter  $\Delta$  decays exponentially which is a signature of the proximity effect that determines the Josephson current in this case. Thus, at the peak condition, the local order parameter  $\Delta$  within the lattice is mostly due to the local interaction, with only a small contribution from the proximity effect seen at the edges.

### C. Finite temperature

The previous results have been obtained at zero temperature  $T = 0$ . We consider in this section the finite temperature case in order to understand the temperature regions where the experiments are potentially performed and seek for the different expected temperature dependence of the critical current

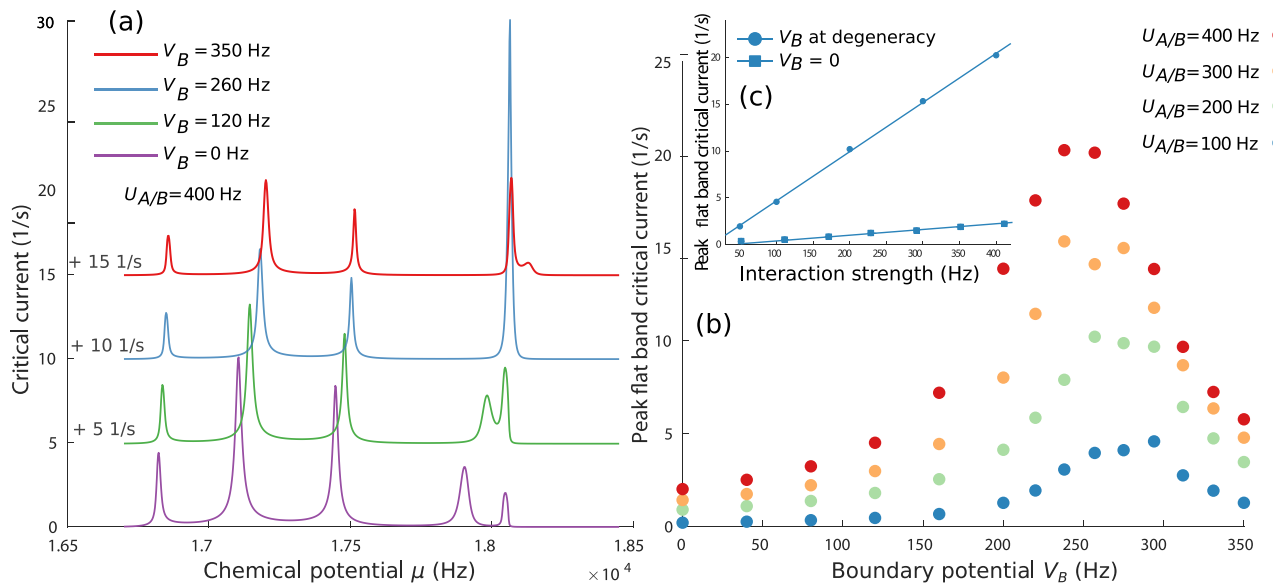


FIG. 3. (a) Critical Josephson current vs chemical potential  $\mu$  for different boundary potentials  $V_B$ . For clarity, the curves have been shifted up as indicated. When  $V_B = 260$  Hz (blue curve) the flat-band current is strongly enhanced. Here,  $\Delta_L = 2.0$  kHz and  $t_C = 1.0$  kHz. (b) The peak critical Josephson current at the flat band versus boundary potential  $V_B$  for different interaction strengths  $U_{A/B}$ . It is seen that the current is maximal around a  $U_{A/B}$ -dependent value of  $V_B$  and beyond that the current begins to decrease. This  $V_B$  value, called the degeneracy value, corresponds to the case in which the bulk flat-band states and the edge states become degenerate in energy. (c) The dependence of the flat-band peak critical Josephson current on the interaction strength  $U_{A/B}$  both when  $V_B$  is tuned at the resonance value and at  $V_B = 0$ . The dependence is found to be linear in both cases but the current is an order of magnitude higher at the degeneracy value of  $V_B$ .

corresponding to the flat-band states and the dispersive band states. The critical temperatures are determined by finding the temperatures at which the critical current vanishes. We consider the situation with the edge potential  $V_B$  tuned to the degeneracy. Otherwise, the parameters are the same as in Fig. 3. The results are shown in Figs. 5(a) and 5(b). It is seen that the critical temperature of the flat-band state is higher than for the dispersive state. Also, the functional dependency of the critical temperature on the interaction is found to be different for dispersive band states and the flat-band states: For flat bands the dependence is linear but for dispersive band states it is not. The critical temperature for dispersive band states is found to be in the range 1–2 nK for the considered interaction strengths, whereas for the flat band it is 2–4 nK.

#### IV. EXPERIMENTAL REALIZATION

Based on the theoretical results shown in Figs. 2–5, we now discuss a possible experimental realization in a mesoscopic cold atom transport experiment. Fermionic lithium-6 is an ideal candidate for probing transport in such structures due to its light mass, which leads to high tunneling rates between lattice sites and tunable interactions from weakly interacting BCS limit to strong interactions (so-called unitarity regime [42,81]). The two leads and the scattering region connecting them can be formed out of a cloud of lithium atoms in a dipole trap by shining two  $\text{TEM}_{01}$  beams of blue-detuned, repulsive light. The resulting channel at the intersection of the two beams' nodal planes (Fig. 6) permits transport between the two leads which is ballistic in the case described or, if an additional potential like a sawtooth lattice is projected into this

region, can have a more complex energy dependence which can be probed by an additional gate beam.

Transport properties of the scattering region such as the conductance or critical current can be measured by preparing a particle number imbalance between the two reservoirs and measuring the particle number in each reservoir as a function of time via absorption imaging. The critical current can then be probed via coherent Josephson oscillations in the particle imbalance in addition to the normal, dissipative flow as the frequency of these oscillations is directly proportional to the square root of the critical current for small particle and phase imbalances [64]. This peculiar dependence of the oscillation frequency on the square root of the critical current is a consequence of the finite size of the reservoirs, as explained in the following. The Josephson relations are  $I = I_c \sin \phi \approx I_c \phi$  and  $\partial_t \phi = \Delta \mu / \hbar$ . The current dynamically changes the particle number imbalance  $I = -\partial_t \Delta N / 2$  which in turn changes the chemical potential imbalance  $\Delta N = \kappa \Delta \mu$  via the compressibility of the reservoirs  $\kappa = (\partial N / \partial \mu)_T$ . Combining these expressions, we obtain the equation

$$\partial_t^2 \Delta N = -(2I_c / \hbar \kappa) \Delta N = -\omega_J^2 \Delta N \quad (22)$$

which gives the Josephson frequency  $\omega_J = \sqrt{2I_c / \hbar \kappa}$ .

The sawtooth lattice can be projected onto the 1D region by holographically shaping an attractive, red-detuned beam with a digital micromirror device (DMD) acting as a spatial light modulator and focusing the beam through a high-resolution microscope [82]. This setup allows us to project many tightly-focused gaussian spots, each acting as a lattice site, with waists on the order of the diffraction limit (approximately  $0.9 \mu\text{m}$ ), an example of which is shown in Fig. 6. For the

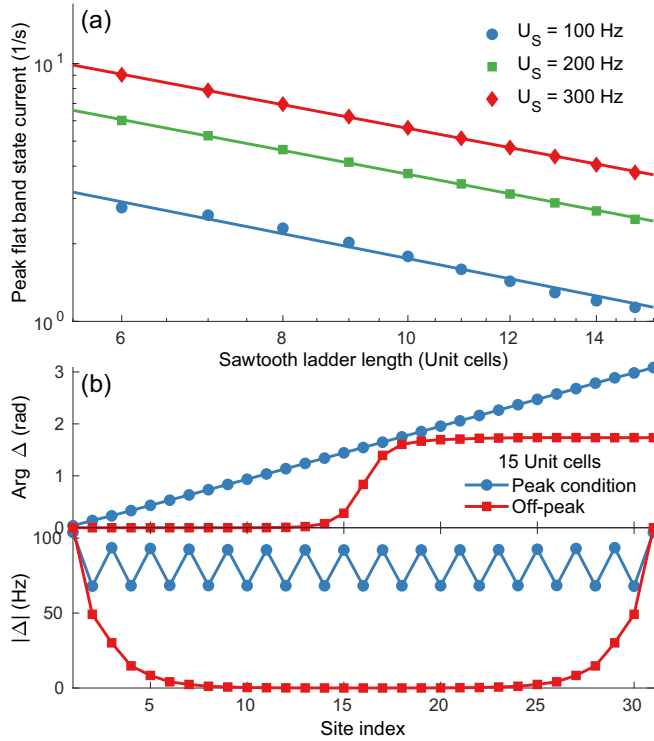


FIG. 4. (a) Dependence of peak flat-band state current on the length of the sawtooth ladder for different interaction strengths  $U_S$ . Here, it is observed that the data follows a power law: The fits  $I \propto N_c^{-\alpha}$ , where  $I$  is the current and  $N_c$  is the number of unit cells, are also shown. The fitted exponents are  $\alpha = 0.99$  for  $U_S = 100$  Hz,  $\alpha = 0.95$  for  $U_S = 200$  Hz, and  $\alpha = 0.95$  for  $U_S = 300$  Hz. (b) The variation of the phase angle and the absolute value of the order parameter  $\Delta$  within the ladder for the condition of maximal flat-band critical current and in the off-peak condition, where the dispersive band states are filled but the flat-band states are empty. The site index increases from the left edge to the right edge of the lattice [check Fig. 1(b)], unit cell by unit cell, the  $A$  sites before  $B$  sites. It is seen that at the peak condition the phase of  $\Delta$  increases linearly from 0 at the left lead to  $\pi$  at the right lead. Since the Josephson current is proportional to the gradient of the phase, this explains the power law behavior observed in Fig. (a). It is also demonstrated that  $\Delta$  within the lattice is mostly due to local interactions instead of the proximity effect, which is instead observed in the off-peak case, where the proximity effect effectively extends the leads into the lattice. The parameters used in (a) and (b) are  $\Delta_L = 2$  kHz and  $t_C = 2$  kHz.

simple case of a set of gaussian spots, the optimal amplitude and phase holograms can be computed analytically, while a sophisticated phase-retrieval algorithm [83] allows us to calculate the optimal holograms for more complex target potentials. Both methods are flexible enough to continuously tune the depth of the boundary sites to bring the edge states into resonance with the flat-band states. For this work, a model sawtooth ladder with three unit cells was simulated to extract experimentally realistic parameters for the tunneling amplitudes provided in Fig. 6. Eventually this will also allow us to further optimize the sawtooth lattice based on the theoretical predictions.

The main challenge in implementing this scheme using cold atoms is the energy scales imposed by the flat band

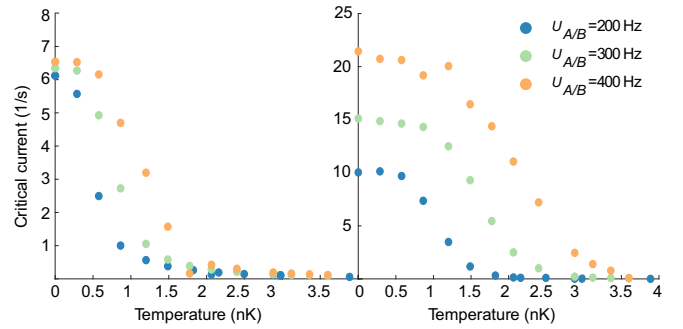


FIG. 5. (a) The peak critical Josephson current dependence on temperature for the dispersive band state with the largest current. The current vanishes around 1–2 nK, depending on the interaction strength  $U_{A/B}$ . (b) The peak critical Josephson current dependence on temperature for the flat-band states. The boundary potential  $V_B$  is set here to the degeneracy value. The current vanishes below measurable amplitude around 2–4 nK, depending on the interaction strength  $U_{A/B}$ . The dependence of the critical current on the temperature and of the critical temperature on the interaction is different for the flat-band states and the dispersive band states.

and the detection sensitivity needed to measure the critical currents. The minimum achievable temperature in the reservoirs is approximately 50 nK which leads to a temperature broadening of the Fermi-Dirac distribution of approximately  $4k_B T = 4.2$  kHz and therefore limits the energy resolution of the transport spectrum to that order of magnitude. Since the transmission peaks between the dispersive and flat-band states are predicted to be separated by only 600 Hz, transport through the flat band cannot be distinguished from transport through the dispersive bands. This means that we must either reduce the temperature or increase the tunneling rate. We can further cool the system by changing the geometry of the

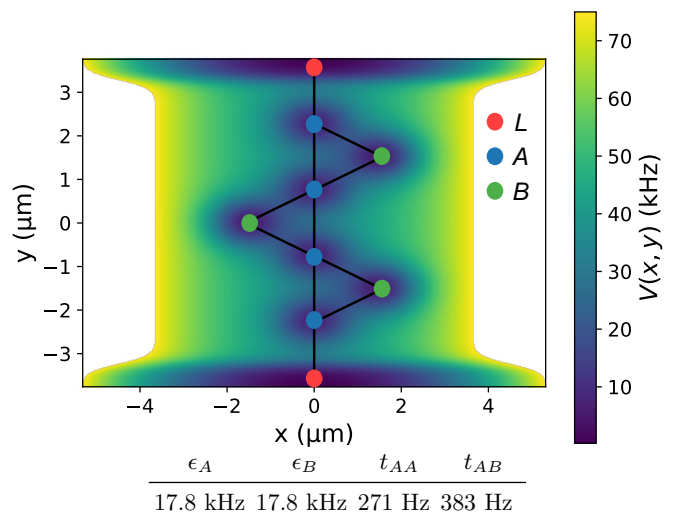


FIG. 6. A possible optical potential for implementing the sawtooth ladder in a two-terminal transport experiment with ultracold gases. The corresponding tight-binding model graph is shown on top of the potential. The tight-binding parameters of the sawtooth lattice shown below are extracted from the potential and have been used to produce all of the results presented in this work.

reservoir trap from harmonic to a uniform box trap whose resulting deconfinement reduces the temperature [84] and would allow us to reach temperatures on the order of 30 nK. A possible method to increase the tunneling rates is to exploit a three-level system present in lithium at high magnetic fields to impose lattices with subwavelength spatial structure [85]. The critical currents predicted in this work are likely below the detection limit of our current experiment though it is possible that measuring the Josephson oscillation frequency instead of the critical currents directly circumvents this problem. However if the oscillations are indeed still too small to resolve, one could measure the normal dissipative transport instead of the DC Josephson effect, i.e., the response to a chemical potential imbalance rather than a phase imbalance. In this way, the strength of the signal—the conductance through the flat-band states—can be increased simply by increasing the imposed chemical potential bias.

## V. DISCUSSION AND CONCLUSION

The strong effect of interactions in a flat (dispersionless) band has been predicted to lead to high critical temperatures of superconductivity [30,31], as well as supercurrents and superfluidity guaranteed by quantum geometric quantities [33,35]. According to theory, in a flat band the critical temperature and the superfluid weight depend linearly on the strength of the interaction that leads to Cooper pair formation; this is a direct signature of the geometric contribution of superconductivity [33,35]. The linear dependence is in striking contrast to the dispersive single band case where the critical temperature is exponentially suppressed and the superfluid weight is only weakly dependent on the interaction. Flat band superconductivity has become topical since the observation of superconductivity in twisted bilayer graphene [23] and other moiré materials [86,87] hosting flat bands. The geometric contribution of superconductivity has been suggested to play a role there [36–39], however, its direct verification is challenging due to the complexity of the moiré materials and limited possibilities of precisely tuning the interaction strength. We proposed here a two-terminal setup to investigate how the salient features of flat-band superconductivity manifest in a transport experiment. Such an experiment can be realized with ultracold gases where the interaction strength is highly controllable and optical lattice potentials that correspond to simple flat-band models can be realized.

We considered a finite-size sawtooth lattice in the channel between two reservoirs and characterized the DC Josephson current. We showed that the linear dependence on the interaction, as expected from the theory for infinite flat-band lattice systems, is visible in the critical current. The experiment we

propose would thus be able to prove the flat-band nature and geometric origin of the superconductivity. The finite size of the lattice manifests itself in an intriguing way: In order to maximize the Josephson current through the bulk flat-band states, one needs to make them degenerate with the boundary states that appear in a finite system and connect the lattice to the leads. Once this energy resonance condition is reached, the critical current and the critical temperature are higher in the flat band than in the dispersive bands, highlighting the general promise of flat-band superconductivity.

Our calculations used parameters obtained from microscopic modeling of real experimental potential landscapes, and we discussed the feasibility of the experiments. It is particularly important that both the interaction and the flat-band state–boundary state energy difference can be easily controlled in the proposed ultracold gas setup. The former is needed for exploring the fundamental properties of flat-band superconductivity, and the latter is useful in verifying that the effects of the finite size of the lattice are well described by the theory presented here. The main challenge in the experimental realization is the temperature scale of the current experiments, which has to be either reduced or made relatively smaller by increasing the hopping energy in the lattice.

Our results show that two-terminal transport experiments, in general, are a promising platform to explore fundamental features of flat-band superconductivity and that ultracold gas transport setups are particularly suited for this. We showed that the finite size of the flat-band lattice system in the transport channel does not prevent observing the most important characteristics of flat-band superconductivity, in contrast, it provides an additional turning knob for the experiments. An interesting future direction is to study also nonequilibrium flat-band transport. The investigation can also be extended to other lattice models such as the railroad-trestle model, realizable as a zigzag lattice [88], and the diamond lattice [89].

## ACKNOWLEDGMENTS

We acknowledge stimulating discussions with Laura Corman, Samuel Häusler, and Martin Lebrat. V.A.J.P., S.P., and P.T. acknowledge support by the Academy of Finland under Projects No. 330384, No. 303351, No. 307419, No. 327293, No. 318987 (QuantERA project RouTe), No. 318937 (PROFI), and by Centre for Quantum Engineering (CQE) at Aalto University. V.A.J.P. acknowledges financial support by the Jenny and Antti Wihuri Foundation. T.E., P.F., and J.M. acknowledge the Swiss National Science Foundation (Grants No. 182650 and No. NCCR-QSIT) and European Research Council advanced grant TransQ (Grant No. 742579) for funding.

- 
- [1] D. Leykam, A. Andreanov, and S. Flach, Artificial flat band systems: from lattice models to experiments, *Adv. Phys.: X* **3**, 1473052 (2018).
- [2] E. H. Lieb, Two Theorems on the Hubbard Model, *Phys. Rev. Lett.* **62**, 1201 (1989).
- [3] A. Mielke, Ferromagnetic ground states for the Hubbard model on line graphs, *J. Phys. A: Math. and Gen.* **24**, L73 (1991).

- [4] A. Mielke, Ferromagnetism in the Hubbard model on line graphs and further considerations, *J. Phys. A: Math. Gen.* **24**, 3311 (1991).
- [5] H. Tasaki, Hubbard model and the origin of ferromagnetism, *Eur. Phys. J. B* **64**, 365 (2008).
- [6] O. Derzhko, J. Richter, and M. Maksymenko, Strongly correlated flat-band systems: the route from Heisenberg spins

- to Hubbard electrons, *Int. J. Mod. Phys. B* **29**, 1530007 (2015).
- [7] N. C. Costa, T. Mendes-Santos, T. Paiva, R. R. dos Santos, and R. T. Scalettar, Ferromagnetism beyond Lieb's theorem, *Phys. Rev. B* **94**, 155107 (2016).
- [8] K. Sun, Z. Gu, H. Katsura, and S. Das Sarma, Nearly Flatbands With Nontrivial Topology, *Phys. Rev. Lett.* **106**, 236803 (2011).
- [9] E. Tang, J.-W. Mei, and X.-G. Wen, High-Temperature Fractional Quantum Hall States, *Phys. Rev. Lett.* **106**, 236802 (2011).
- [10] T. Neupert, L. Santos, C. Chamon, and C. Mudry, Fractional Quantum Hall States at Zero Magnetic Field, *Phys. Rev. Lett.* **106**, 236804 (2011).
- [11] A. Zhao and S.-Q. Shen, Quantum anomalous Hall effect in a flat band ferromagnet, *Phys. Rev. B* **85**, 085209 (2012).
- [12] B. Jaworowski, A. Manolescu, and P. Potasz, Fractional chern insulator phase at the transition between checkerboard and Lieb lattice, *Phys. Rev. B* **92**, 245119 (2015).
- [13] C. Wu, D. Bergman, L. Balents, and S. Das Sarma, Flat Bands and Wigner Crystallization in the Honeycomb Optical Lattice, *Phys. Rev. Lett.* **99**, 070401 (2007).
- [14] G.-B. Jo, J. Guzman, C. K. Thomas, P. Hosur, A. Vishwanath, and D. M. Stamper-Kurn, Ultracold Atoms in a Tunable Optical Kagome Lattices, *Phys. Rev. Lett.* **108**, 045305 (2012).
- [15] S. Taie, H. Ozawa, T. Ichinose, T. Nishio, S. Nakajima, and Y. Takahashi, Coherent driving and freezing of bosonic matter wave in an optical Lieb lattice, *Sci. Adv.* **1**, e1500854 (2015).
- [16] T.-H. Leung, M. N. Schwarz, S.-W. Chang, C. D. Brown, G. Unnikrishnan, and D. Stamper-Kurn, Interaction-Enhanced Group Velocity of Bosons in the Flat Band of an Optical Kagome Lattice, *Phys. Rev. Lett.* **125**, 133001 (2020).
- [17] H. Gersen, T. J. Karle, R. J. P. Engelen, W. Bogaerts, J. P. Korterik, N. F. van Hulst, T. F. Krauss, and L. Kuipers, Real-space Observation of Ultraslow Light in Photonic Crystal Waveguides, *Phys. Rev. Lett.* **94**, 073903 (2005).
- [18] S. Mukherjee, A. Spracklen, D. Choudhury, N. Goldman, P. Íhberg, E. Anderson, and R. R. Thomson, Observation of Localized Flat-band State in a Photonic Lieb Lattice, *Phys. Rev. Lett.* **114**, 245504 (2015).
- [19] R. A. Vicencio, C. Cantillano, L. Morales-Inostroza, B. Real, C. Mejía-Cortés, S. Weimann, A. Szameit, and M. I. Molina, Observation of Localized States in Lieb Photonic Lattices, *Phys. Rev. Lett.* **114**, 245503 (2015).
- [20] S. Weimann, L. Morales-Inostroza, B. Real, C. Cantillano, A. Szameit, and R. A. Vicencio, Transport in sawtooth photonic lattices, *Opt. Lett.* **41**, 2414 (2016).
- [21] H. S. Nguyen, F. Dubois, T. Deschamps, S. Cuff, A. Pardon, J.-L. Leclercq, C. Seassal, X. Letartre, and P. Viktorovitch, Symmetry Breaking in Photonic Crystals: On-demand Dispersion From Flatband to Dirac cones, *Phys. Rev. Lett.* **120**, 066102 (2018).
- [22] T. Jacqmin, I. Carusotto, I. Sagnes, M. Abbarchi, D. D. Solnyshkov, G. Malpuech, E. Galopin, A. Lemaître, J. Bloch, and A. Amo, Direct Observation of Dirac Cones and a Flatband in a Honeycomb Lattice for Polaritons, *Phys. Rev. Lett.* **112**, 116402 (2014).
- [23] Y. Cao, V. Fatemi, S. Fang, K. Watanabe, T. Taniguchi, E. Kaxiras, and P. Jarillo-Herrero, Unconventional superconductivity in magic-angle graphene superlattices, *Nature (London)* **556**, 43 (2018).
- [24] D. Marchenko, D. V. Evtushinsky, E. Golias, A. Varykhalov, T. Seyller, and O. Rader, Extremely flat band in bilayer graphene, *Sci. Adv.* **4**, eaau0059 (2018).
- [25] Z. Li, J. Zhuang, L. Wang, H. Feng, Q. Gao, X. Xu, W. Hao, X. Wang, C. Zhang, K. Wu, S. X. Dou, L. Chen, Z. Hu, and Y. Du, Realization of flat band with possible nontrivial topology in electronic kagome lattice, *Sci. Adv.* **4**, eaau4511 (2018).
- [26] H. C. Po, L. Zou, A. Vishwanath, and T. Senthil, Origin of Mott Insulating Behavior and Superconductivity in Twisted Bilayer Graphene, *Phys. Rev. X* **8**, 031089 (2018).
- [27] R. Drost, T. Ojanen, A. Harju, and P. Liljeroth, Topological states in engineered atomic lattices, *Nat. Phys.* **13**, 668 (2017).
- [28] M. R. Slot, T. S. Gardenier, P. H. Jacobse, G. C. P. van Miert, S. N. Kempkes, S. J. M. Zevenhuizen, C. M. Smith, D. Vanhaeckelbergh, and I. Swart, Experimental realization and characterization of an electronic Lieb lattice, *Nat. Phys.* **13**, 672 (2017).
- [29] M. N. Huda, S. Kezilebieke, and P. Liljeroth, Designer flat bands in quasi-one-dimensional atomic lattices, *Phys. Rev. Research* **2**, 043426 (2020).
- [30] N. B. Kopnin, T. T. Heikkilä, and G. E. Volovik, High-temperature surface superconductivity in topological flat-band systems, *Phys. Rev. B* **83**, 220503(R) (2011).
- [31] T. T. Heikkilä, N. B. Kopnin, and G. E. Volovik, Flat bands in topological media, *JETP Lett.* **94**, 233 (2011).
- [32] B. Uchoa and Y. Barlas, Superconducting States in Pseudo-Landau-Levels of Strained Graphene, *Phys. Rev. Lett.* **111**, 046604 (2013).
- [33] S. Peotta and P. Törmä, Superfluidity in topologically nontrivial flat bands, *Nat. Commun.* **6**, 8944 (2015).
- [34] A. Julku, S. Peotta, T. I. Vanhala, D.-H. Kim, and P. Törmä, Geometric Origin of Superfluidity in the Lieb-lattice Flat Band, *Phys. Rev. Lett.* **117**, 045303 (2016).
- [35] L. Liang, T. I. Vanhala, S. Peotta, T. Siro, A. Harju, and P. Törmä, Band geometry, berry curvature and superfluid weight, *Phys. Rev. B* **95**, 024515 (2017).
- [36] A. Julku, T. Peltonen, L. Liang, T. Heikkilä, and P. Törmä, Superfluid weight and berezinskii-kosterlitz-thouless transition temperature of twisted bilayer graphene, *Phys. Rev. B* **101**, 060505(R) (2020).
- [37] X. Hu, T. Hyart, D. I. Pikulin, and E. Rossi, Geometric and Conventional Contribution to the Superfluid Weight in Twisted Bilayer Graphene, *Phys. Rev. Lett.* **123**, 237002 (2019).
- [38] F. Xie, Z. Song, B. Lian, and B. A. Bernevig, Topology-Bounded Superfluid Weight in Twisted Bilayer Graphene, *Phys. Rev. Lett.* **124**, 167002 (2020).
- [39] L. Classen, Geometry rescues superconductivity in twisted graphene, *Physics* **13**, 23 (2020).
- [40] F. Wu, A. H. MacDonald, and I. Martin, Theory of Phonon-mediated Superconductivity in Twisted Bilayer Graphene, *Phys. Rev. Lett.* **121**, 257001 (2018).
- [41] B. A. Bernevig, B. Lian, A. Cowsik, F. Xie, N. Regnault, and Z.-D. Song, TBG V: Exact analytic many-body excitations in twisted bilayer graphene coulomb hamiltonians:

- Charge gap, goldstone modes and absence of cooper pairing, [arXiv:2009.14200](https://arxiv.org/abs/2009.14200).
- [42] P. Törmä and K. Sengstock (Eds.), *Quantum Gas Experiments, Exploring Many-Body States* (World Scientific, London, 2014).
- [43] M. Schulze, D. Bercioux, and D. F. Urban, Adiabatic pumping in the quasi-one-dimensional triangle lattice, *Phys. Rev. B* **87**, 024301 (2013).
- [44] M. Johansson, U. Naether, and R. A. Vicencio, Compactification tuning for nonlinear localized modes in sawtooth lattices, *Phys. Rev. E* **92**, 032912 (2015).
- [45] S. Datta, *Electronic Transport in Mesoscopic Systems* (Cambridge University Press, Cambridge, 1995).
- [46] J.-P. Brantut, J. Meineke, D. Stadler, S. Krinner, and T. Esslinger, Conduction of ultracold fermions through a mesoscopic channel, *Science* **337**, 1069 (2012).
- [47] S. Krinner, D. Stadler, D. Husmann, J.-P. Brantut, and T. Esslinger, Observation of quantized conductance in neutral matter, *Nature (London)* **517**, 64 (2015).
- [48] D. Husmann, S. Uchino, S. Krinner, M. Lebrat, T. Giamarchi, T. Esslinger, and J.-P. Brantut, Connecting strongly correlated superfluids by a quantum point contact, *Science* **350**, 1498 (2015).
- [49] M. Lebrat, P. Grišin, D. Husmann, S. Häusler, L. Corman, T. Giamarchi, J.-P. Brantut, and T. Esslinger, Band and Correlated Insulators of Cold Fermions in a Mesoscopic Lattice, *Phys. Rev. X* **8**, 011053 (2018).
- [50] S. Krinner, T. Esslinger, and J.-P. Brantut, Two-terminal transport measurements with cold atoms, *J. Phys.: Condens. Matter* **29**, 343003 (2017).
- [51] L. Amico, G. Birkel, M. Boshier, and L.-C. Kwek, Focus on atomtronics-enabled quantum technologies, *New J. Phys.* **19**, 020201 (2017).
- [52] L. Amico, M. Boshier, G. Birkel, A. Minguzzi, C. Miniatura, L. C. Kwek, D. Aghamalyan, V. Ahufinger, N. Andrei, A. S. Arnold, M. Baker, T. A. Bell, T. Bland, J. P. Brantut, D. Cassettari, F. Chevy, R. Citro, S. D. Palo, R. Dumke, M. Edwards, R. Folman, J. Fortagh, S. A. Gardiner, B. M. Garraway, G. Gauthier, A. Günther, T. Haug, C. Hufnagel, M. Keil, W. von Klitzing, P. Ireland, M. Lebrat, W. Li, L. Longchambon, J. Mompart, O. Morsch, P. Naldesi, T. W. Neely, M. Olshanii, E. Orignac, S. Pandey, A. Pérez-Obiol, H. Perrin, L. Piroli, J. Polo, A. L. Pritchard, N. P. Proukakis, C. Rylands, H. Rubinsztein-Dunlop, F. Scazza, S. Stringari, F. Tosto, A. Trombettoni, N. Victorin, D. Wilkowski, K. Khani, and A. Yakimenko, Roadmap on atomtronics, [arXiv:2008.04439](https://arxiv.org/abs/2008.04439).
- [53] S. D. Huber and E. Altman, Bose condensation in flat bands, *Phys. Rev. B* **82**, 184502 (2010).
- [54] T. Zhang and G.-B. Jo, One-dimensional sawtooth and zigzag lattices for ultracold atoms, *Sci. Rep.* **5**, 16044 (2015).
- [55] B. Sutherland, Localization of electronic wave functions due to local topology, *Phys. Rev. B* **34**, 5208 (1986).
- [56] B. D. Josephson, Possible new effects in superconductive tunneling, *Phys. Lett.* **1**, 251 (1962).
- [57] V. Meden, The Anderson-Josephson quantum dot - a theory perspective, *J. Phys.: Condens. Matter* **31**, 163001 (2019).
- [58] D. J. Scalapino, S. R. White, and S. C. Zhang, Superfluid Density and the Drude Weight of the Hubbard Model, *Phys. Rev. Lett.* **68**, 2830 (1992).
- [59] D. J. Scalapino, S. R. White, and S. C. Zhang, Insulator, metal, or superconductor: The criteria, *Phys. Rev. B* **47**, 7995 (1993).
- [60] M. Tovmasyan, S. Peotta, L. Liang, P. Törmä, and S. D. Huber, Preformed pairs in flat Bloch bands, *Phys. Rev. B* **98**, 134513 (2018).
- [61] F. S. Cataliotti, S. Burger, C. Fort, P. Maddaloni, F. Minardi, A. Trombettoni, A. Smerzi, and M. Inguscio, Josephson junction arrays with Bose-Einstein condensates, *Science* **293**, 843 (2001).
- [62] M. Albiez, R. Gati, J. Fölling, S. Hunsmann, M. Cristiani, and M. K. Oberthaler, Direct Observation of Tunneling and Nonlinear Self-trapping in a Single Bosonic Josephson Junction, *Phys. Rev. Lett.* **95**, 010402 (2005).
- [63] S. Levy, E. Lahoud, I. Shomroni, and J. Steinhauer, The a.c. and d.c. Josephson effects in a Bose-Einstein condensate, *Nature (London)* **449**, 579 (2007).
- [64] G. Valtolina, A. Burchianti, A. Amico, E. Neri, K. Khani, J. A. Seman, A. Trombettoni, A. Smerzi, M. Zaccanti, M. Inguscio, and G. Roati, Josephson effect in fermionic superfluids across the BEC-BCS crossover, *Science* **350**, 1505 (2015).
- [65] T. Betz, S. Manz, R. Bücke, T. Berrada, C. Koller, G. Kazakov, I. E. Mazets, H.-P. Stimming, A. Perrin, T. Schumm, and J. Schmiedmayer, Two-point Phase Correlations of a One-dimensional Bosonic Josephson Junction, *Phys. Rev. Lett.* **106**, 020407 (2011).
- [66] C. Ryu, P. W. Blackburn, A. A. Blinova, and M. G. Boshier, Experimental Realization of Josephson Junctions for an Atom Squid, *Phys. Rev. Lett.* **111**, 205301 (2013).
- [67] G. Spagnolli, G. Semeghini, L. Masi, G. Ferioli, A. Trenkwalder, S. Coop, M. Landini, L. Pezzè, G. Modugno, M. Inguscio, A. Smerzi, and M. Fattori, Crossing over From Attractive to Repulsive Interactions in a Tunneling Bosonic Josephson Junction, *Phys. Rev. Lett.* **118**, 230403 (2017).
- [68] A. Burchianti, F. Scazza, A. Amico, G. Valtolina, J. A. Seman, C. Fort, M. Zaccanti, M. Inguscio, and G. Roati, Connecting Dissipation and Phase Slips in a Josephson Junction Between Fermionic Superfluids, *Phys. Rev. Lett.* **120**, 025302 (2018).
- [69] N. Luick, L. Sobirey, M. Bohlen, V. P. Singh, L. Mathey, T. Lompe, and H. Moritz, An ideal Josephson junction in an ultracold two-dimensional Fermi gas, *Science* **369**, 89 (2020).
- [70] W. J. Kwon, G. Del Pace, R. Panza, M. Inguscio, W. Zwerger, M. Zaccanti, F. Scazza, and G. Roati, Strongly correlated superfluid order parameters from dc Josephson supercurrents, *Science* **369**, 84 (2020).
- [71] M. Tovmasyan, S. Peotta, P. Törmä, and S. D. Huber, Effective theory and emergent SU(2) symmetry in the flat bands of attractive Hubbard models, *Phys. Rev. B* **94**, 245149 (2016).
- [72] C. Yang, W. Gao, and J. C. Meza, On the convergence of the self-consistent field iteration for a class of nonlinear eigenvalue problems, *SIAM J. Matrix Anal. Appl.* **30**, 4 (2008).
- [73] C. G. Broyden, A class of methods for solving nonlinear simultaneous equations, *Math. Comp.* **19**, 577 (1965).
- [74] D. G. Anderson, Iterative procedures for nonlinear integral equations, *JACM* **12**, 547 (1965).
- [75] P. Pulay, Improved scf convergence acceleration, *J. Comput. Chem.* **3**, 556 (1982).
- [76] A. M. Black-Schaffer and S. Doniach, Self-consistent solution for proximity effect and Josephson current in ballistic graphene SNS Josephson junctions, *Phys. Rev. B* **78**, 024504 (2008).

- [77] A. Martín-Rodero and A. L. Yeyati, Josephson and Andreev transport through quantum dots, *Adv. Phys.* **60**, 899 (2011).
- [78] P. Törmä, L. Liang, and S. Peotta, Quantum metric and effective mass of a two-body bound state in a flat band, *Phys. Rev. B* **98**, 220511(R) (2018).
- [79] C. Ishii, Josephson currents through junctions with normal metal barriers, *Prog. Theor. Phys.* **44**, 1525 (1970).
- [80] J. Bardeen and J. L. Johnson, Josephson current flow in pure superconducting-normal-superconducting junctions, *Phys. Rev. B* **5**, 72 (1972).
- [81] W. Zwerger editor, *The BCS-BEC Crossover and the Unitary Fermi Gas*, Lecture Notes in Physics Vol. 836 (Springer-Verlag, Berlin, Heidelberg, 2012).
- [82] P. Zupancic, P. M. Preiss, R. Ma, A. Lukin, M. E. Tai, M. Rispoli, R. Islam, and M. Greiner, Ultra-precise holographic beam shaping for microscopic quantum control, *Opt. Express* **24**, 13881 (2016).
- [83] M. Pasienski and B. DeMarco, A high-accuracy algorithm for designing arbitrary holographic atom traps, *Opt. Express* **16**, 2176 (2008).
- [84] G. Su, J. Chen, and L. Chen, Low-temperature behavior of a weakly interacting Fermi gas trapped in a power-law potential, *Phys. Lett. A* **315**, 109 (2003).
- [85] Y. Wang, S. Subhankar, P. Bienias, M. Łaacki, T.-C. Tsui, M. A. Baranov, A. V. Gorshkov, P. Zoller, J. V. Porto, and S. L. Rolston, Dark State Optical Lattice With a Sub-wavelength Spatial Structure, *Phys. Rev. Lett.* **120**, 083601 (2018).
- [86] C. Shen, Y. Chu, Q. Wu, N. Li, S. Wang, Y. Zhao, J. Tang, J. Liu, J. Tian, K. Watanabe, T. Taniguchi, R. Yang, Z. Y. Meng, D. Shi, O. V. Yazyev, and G. Zhang, Correlated states in twisted double bilayer graphene, *Nat. Phys.* **16**, 520 (2020).
- [87] X. Liu, Z. Hao, E. Khalaf, J. Y. Lee, Y. Ronen, H. Yoo, D. H. Najafabadi, K. Watanabe, T. Taniguchi, A. Vishwanath, and P. Kim, Tunable spin-polarized correlated states in twisted double bilayer graphene, *Nature (London)* **583**, 221 (2020).
- [88] K. Kuroki, R. Arita, and H. Aoki, Numerical study of a superconductor-insulator transition in a half-filled hubbard chain with distant transfers, *J. Phys. Soc. Jpn.* **66**, 3371 (1997).
- [89] K. Kobayashi, M. Okumura, S. Yamada, M. Machida, and H. Aoki, Superconductivity in repulsively interacting fermions on a diamond chain: Flat-band-induced pairing, *Phys. Rev. B* **94**, 214501 (2016).